

# The Na I D resonance lines in main sequence late-type stars

Rodrigo F. Díaz, Carolina Cincunegui and Pablo J. D. Mauas

*Instituto de Astronomía y Física del Espacio, CC. 67, suc. 28, 1428. Buenos Aires, Argentina.*

3 October 2018

## ABSTRACT

We study the sodium D lines (D1: 5895.92 Å; D2: 5889.95 Å) in late-type dwarf stars. The stars have spectral types between F6 and M5.5 ( $B-V$  between 0.457 and 1.807) and metallicity between  $[Fe/H] = -0.82$  and 0.6. We obtained medium resolution *echelle* spectra using the 2.15-m telescope at the argentinian observatory CASLEO. The observations have been performed periodically since 1999. The spectra were calibrated in wavelength and in flux. A definition of the pseudo-continuum level is found for all our observations. We also define a continuum level for calibration purposes. The equivalent width of the D lines is computed in detail for all our spectra and related to the colour index ( $B - V$ ) of the stars. When possible, we perform a careful comparison with previous studies. Finally, we construct a spectral index ( $R'_D$ ) as the ratio between the flux in the D lines, and the bolometric flux. We find that, once corrected for the photospheric contribution, this index can be used as a chromospheric activity indicator in stars with a high level of activity. Additionally, we find that combining some of our results, we obtain a method to calibrate in flux stars of unknown colour.

**Key words:** Stars: late-type - Stars: activity - Stars: chromospheres

## 1 INTRODUCTION

All through the main sequence, the Na I D resonance lines (D1: 5895.92 Å; D2: 5889.95 Å) are ubiquitous absorption features, clearly visible in stars of all spectral types. In particular, for cool stars at the end of the main sequence (late G, K and M) the doublet develops strong absorption wings. In the most active flare stars, the D lines show chromospheric emission in their core, a telltale of collision dominated formation processes.

Besides the intrinsic interest in understanding how these lines behave for different stellar parameters, the sodium doublet provides a useful diagnostic tool when studying stellar atmospheres. In this regard, Andretta et al. (1997), Short & Doyle (1998) and Mauas (2000) showed that in M dwarfs the sodium D lines provide information of the conditions in the middle-to-lower chromosphere, and therefore complements the diagnostics of the upper-chromosphere and low transition region provided by H $\alpha$ . Tripicchio et al. (1997) modelled the equivalent width of the doublet in stars of a wide range of spectral types (between F6 and M5.5). They concluded that the chromosphere is not very important in determining the equivalent width, since it only affects emission in the central core, which provides a small contribution to the doublet strength. However, their model fails to reproduce the tendency shown by their observations for stars with  $T_{eff} < 4000^\circ K$ .

In the present work we study different features of the D lines using medium resolution *echelle* spectra covering the entire visible spectrum. Our study is focused on stars at the end of the main sequence (from late F to middle M), for which we analyze the continuum and line fluxes and the equivalent width of the doublet.

In Sect. 2 we describe the observations and calibration pro-

cess. In Sect. 3 we study the continuum flux near the D lines. The equivalent width is treated in Sect. 4, where we also describe a method to obtain an approximate flux calibration for stars of unknown colour index. In Sect. 5 we study the changes observed in the D lines as a consequence of chromospheric activity. Finally, in Sect. 6 we discuss the results and present our conclusions.

## 2 OBSERVATIONS AND STELLAR SAMPLE

### 2.1 Observations and calibration of the spectra

The observations were obtained at the Complejo Astronómico El Leoncito (CASLEO), in the province of San Juan, Argentina, in 27 observing runs starting in March 1999. At present, the spectra of only 19 of these runs were reduced and calibrated.

We used the 2.15-m telescope, equipped with a REOSC *echelle* spectrograph designed to work between 3500 Å and 7500 Å. As a detector we used a 1024 x 1024 pixel TEK CCD.

We obtained spectra covering the whole region between 3860 and 6690 Å, which lies in 24 *echelle* orders. Due to this complete coverage we can study the effect of chromospheric activity in all the optical spectrum simultaneously. In the present work we concentrate on the sodium D lines. The study of other lines is done somewhere else (see Cincunegui et al. 2006; Buccino & Mauas 2007).

We used a 300  $\mu m$ -width slit which provided a resolving power of  $R = \lambda/\delta\lambda \approx 26400$ . This corresponds to a spectral resolution of around 0.22 Å at the centre of the D doublet. Additionally, we obtained ThAr spectra for the wavelength calibration and medium resolution long slit spectra that were employed for the flux calibration.

The observations were reduced and extracted using standard IRAF<sup>1</sup> routines. The details of the flux calibration process are presented in Cincunegui & Mauas (2004).

## 2.2 Stellar sample

Since 1999 we have been monitoring around 110 stars of the main sequence on a regular basis. Each star was observed around three times a year, weather permitting.

The stellar sample is presented in Table 4. The stars have spectral types between F6 and M5.5 and colour indexes ( $B - V$ ) between 0.457 and 1.807, from the Hipparcos/Tycho catalogues (Perryman et al. 1997; Hoeg et al. 1997). The metallicity was obtained from different sources, as shown in Table 4 and range from  $[Fe/H] = -0.82$  to 0.6.

The sample was gathered for different research programmes. All the stars are field stars, and were included either for being similar to the Sun, for exhibiting high levels of chromospheric activity -as is usually the case for the M stars-, or for having planetary companions. We have also observed a few sub-giant stars for calibration purposes, which were excluded from the present analysis. In previous works we used 18 of the stars included in the sample to calibrate the S index calculated at CASLEO (Cincunegui & Mauas 2002; Cincunegui et al. 2006) to the one obtained at Mount Wilson (Vaughan et al. 1978). These 18 stars also belong to the group of standard stars used by Henry et al. (1996) at Cerro Tololo. Several stars were included to cover the entire range of effective temperature. However, the sample is not uniform in metallicity or effective temperature. Nevertheless, we believe our results are not biased by this lack of uniformity in our sample. When such a risk is present, we binned the observations (see Sect. 3).

Our sample also includes seven stars that fall outside the main sequence when placed in an HR diagram, even though they are classified as dwarf stars in the SIMBAD<sup>2</sup> database. For these stars, we calculated the absolute magnitude in the V filter ( $M_V$ ) using the measurements of parallax and V from the Hipparcos/Tycho catalogues (Perryman et al. 1997; Hoeg et al. 1997). We list these stars in Table 1. The fourth column shows the luminosity class that corresponds to the calculated  $M_V$  (see Allen 1964, §95), obtained assuming that the spectral type is correct. These stars were excluded from the analysis, together with the rest of the non-main-sequence stars.

Also contained in our sample are four stars which are listed in a luminosity class other than V in the SIMBAD database that actually fall well within the main sequence. Again,  $M_V$  values were obtained and compared with the table in Allen (1964) to confirm their placement in the HR diagram. These stars are shown in Table 2, and were included in the analysis. We also excluded from the analysis the stars with unknown parallax, since for them absolute fluxes cannot be determined. Our final sample consists of 652 spectra for 84 stars.

	Spectral type	( $B - V$ )	$M_V$	Lum Class
hd103112	K0	1.05	3.18	IV
hd105115	K2/K3	1.41	-0.68	III
hd119285	K1p	1.04	3.39	IV
hd25069	G9	0.99	2.75	IV
hd5869	K4	1.49	1.05	III
hd94683	K4	1.78	-2.38	II
hd17576	G0	1.78	1.91	III

**Table 1.** Stars located outside the main sequence in an HR diagram despite being classified as dwarf-type stars. The fourth column is the luminosity class we obtained assuming the spectral type is correct

Star	Spectral type (SIMBAD)	( $B - V$ )	$M_V$
hd52265	G0 III-IV	0.57	4.12
hd57555	GO IV/V	0.66	4.18
hd75289	G0 I	0.58	4.1
hd120136	F6 IV	0.51	3.58

**Table 2.** Stars located in the main sequence despite not being classified as dwarf-type stars.

## 3 PSEUDO-CONTINUUM

### 3.1 Definition

In Fig. 1 we show the spectrum in the region of the D lines for four stars of different spectral types. As can be seen in the spectra, in the case of later stars the doublet forms inside a strong molecular band, which extends from 5847 Å to 6058 Å and is due to TiO (Mauas & Falchi 1994)

Therefore, in order to obtain a reliable estimate of the continuum flux near the lines for all spectral types, the windows chosen have to be located far away from the line centre, outside the molecular bands. The closest regions are a 10 Å wide window centered at 5805 Å (window V) and a 20 Å wide window centered at 6090 Å (window R). These windows are indicated in Fig. 1 with solid lines.

However, even in these regions there are several photospheric lines, and therefore computing the mean flux would lead to a considerable underestimation of the continuum flux. To deal with this problem, we considered the mean value of the ten highest points in each window as an indication of the continuum flux in it. Finally, to take into account the shape of the continuum in this region, we computed the flux at the doublet centre ( $F_{cont}$ ) as the linear interpolation of the values in each window.

In Fig. 1, the linear interpolation in each spectrum is shown as a dashed line. We see that this is a good estimation for the continuum flux at the centre of the doublet, even for M-type stars.

### 3.2 Relation with (B-V)

We calculated  $F_{cont}$  for all the spectra in our sample in the way explained above.  $F_{cont}$  was normalized to the flux  $F_{\odot}$ , defined in such a way that  $F_{cont}/F_{\odot} = 1$  for a star of solar colour ( $B - V$ ) = 0.62. In Fig. 2 we plot  $F_{cont}/F_{\odot}$  in logarithmic scale as a function of colour index ( $B - V$ ). The trend is similar to that shown by the lower end of the main sequence in an HR diagram.

<sup>1</sup> IRAF is distributed by the National Optical Astronomy Observatories, which are operated by the Association of Universities for Research in Astronomy, Inc., under cooperative agreement with the National Science Foundation.

<sup>2</sup> <http://simbad.u-strasbg.fr>

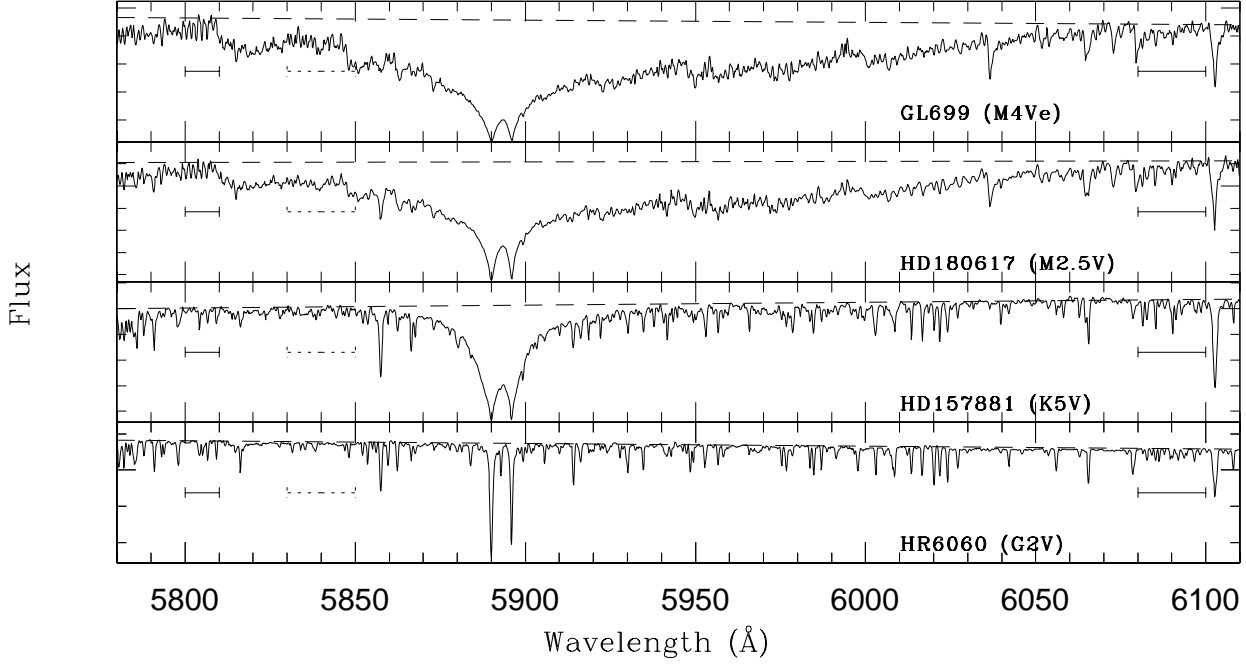


**Figure 1.** The region of the sodium doublet for stars of different spectral types. The dotted lines mark the windows used for the calculation of the continuum flux. The dashed line is the continuum level as defined in Sect. 3.1.

As can be seen in Fig. 2, the stars are not evenly distributed with colour, a fact that might bias our results. To avoid this, we binned the observations every 0.05 units in  $(B - V)$ . For each bin, we computed the mean value of  $F_{cont}$ , which are plotted as filled squares in Fig. 2. It can be seen in the figure that there exists a break at  $(B - V) = 1.4$ , where M stars begin. Therefore, we fitted the binned data with two linear relations:

$$\log\left(\frac{F_{cont}}{F_{\odot}}\right) = \begin{cases} 1.18 - 1.86 \times (B - V) & (B - V < 1.4) \\ 7.55 - 6.55 \times (B - V) & (B - V \geq 1.4) \end{cases} \quad (1)$$

where  $F_{\odot} = 5.7334 \times 10^{-11} \text{ erg cm}^{-2} \text{ s}^{-1} \text{ Å}^{-1}$ .

### 3.3 Calibration

A relation like that of Eq. 1 can be used to calibrate in flux spectra of stars of known colour index  $(B - V)$ . However, most spectrographs only observe a small wavelength range around the line of interest. For these instruments, the windows at 5805 Å and 6010 Å might fall outside the observed range. For this reason, we studied a relation similar to the one in Eq. 1 for a continuum window closer to the doublet.

First, we note that due to the presence of molecular bands, the raw spectra of M-type stars are difficult to normalize, in particular if the observed range is not wide enough. Therefore, we did not try to find a good pseudo-continuum to calibrate M-dwarfs. For F, G and K stars, we considered a window 20 Å wide around 5840 Å, which is indicated in Fig. 1 with dotted lines.

In Fig. 3 we show the ratio between the mean flux  $\bar{F}$  in this window and the one obtained earlier, for stars with  $(B - V) < 1.4$ . As can be seen, using  $\bar{F}$  underestimates the true continuum, but

the percentual difference between both is smaller than 6 per cent. Therefore, the first part of Eq. 1 can be used to fit the mean flux  $\bar{F}$ , and to calibrate in flux this region of the spectrum of a star of known  $(B - V)$ , increasing the error by less than 6 per cent.

## 4 EQUIVALENT WIDTH

### 4.1 Definition

The equivalent width  $W_{\lambda}$  of a spectral line is defined as

$$W_{\lambda} = \int_{\lambda_1}^{\lambda_2} \left(1 - \frac{F_{\lambda}}{F_c}\right) d\lambda, \quad (2)$$

where  $F_c$  is the continuum flux and  $F_{\lambda}$  is the value of the flux in the line. As we pointed out in the preceeding section, the choice of the continuum level can be subjective, and it can be very difficult for M-dwarfs.

On the other hand, the limits of the wings of a line are not always well-defined, and therefore the integration limits  $\lambda_1$  and  $\lambda_2$  also constitute subjective points in the definition of  $W_{\lambda}$ . In fact, while in earlier F and G stars the photospheric wings are thin and well defined, in later stars the wings are extremely wide. Therefore, the choice of a proper integration window requires a varying width ( $\Delta\lambda = \lambda_2 - \lambda_1$ ), ranging from 14 to 40 Å around the centre of the doublet (5892.94 Å), depending on the spectral type of the star. In Table 3 we list the values of  $\Delta\lambda$  we used for different colours. A similar technique, with varying widths, was used by Tripicchio et al. (1997), although it is not clear from their paper which  $\Delta\lambda$  was used for each colour.

Note that in stars with spectral type later than M2.5 the absorption wings of the D lines become very large and blended with

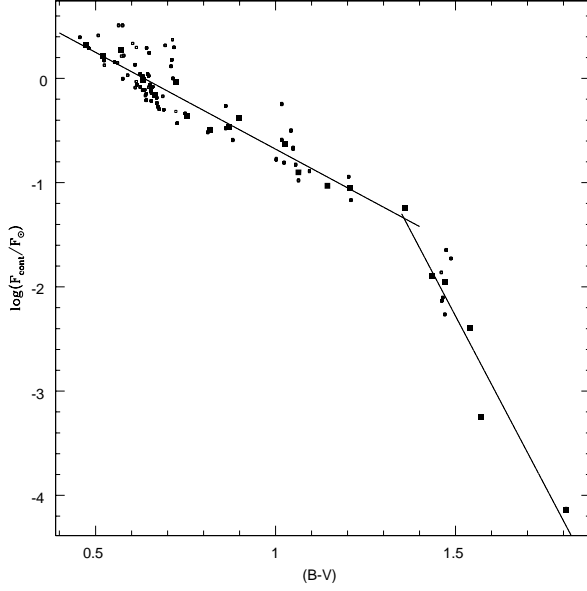


**Figure 2.**  $\log(F_{\text{cont}}/F_{\odot})$  vs. colour index  $(B - V)$ . The small empty squares represent the individual observations, and the filled squares are the mean value in each bin (see text). The solid lines are the best piecewise fit to the data. Note that in several bins there is only one star, and the individual observations are therefore hidden by the filled square.

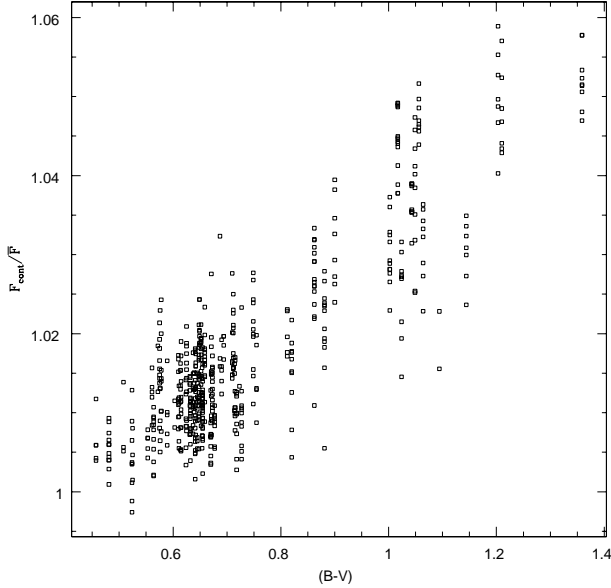


**Figure 3.** Ratio between  $F_{\text{cont}}$  and the mean flux  $\bar{F}$  in the 5830-5850 Å window, as a function of colour index  $(B - V)$ . The percentage difference remains smaller than 6 per cent for F, G and K stars.

the highly-developed absorption bands present (see Fig. 1). Therefore, for these stars a suitable choice of  $\Delta\lambda$  is very difficult and the calculation of the equivalent width cannot be considered entirely reliable.

Regarding the continuum level, we used both values described in the previous section. The equivalent width computed with  $\bar{F}$ ,

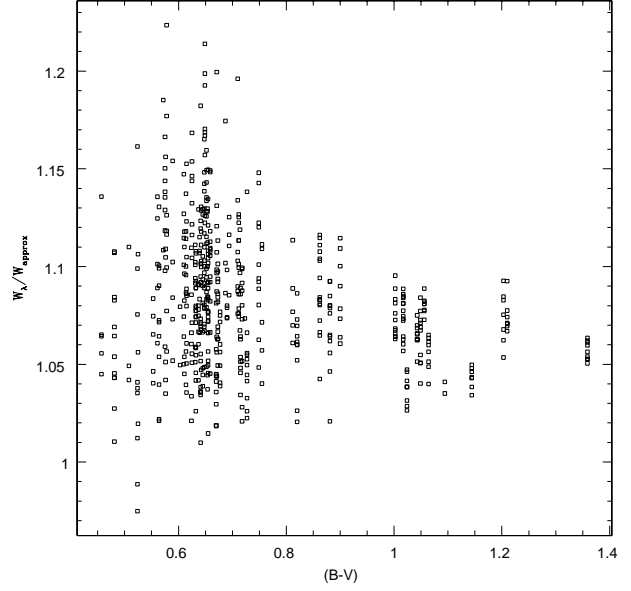


**Figure 4.** Ratio between  $W_{\lambda}$ , calculated with a realistic estimation of the continuum flux ( $F_c = F_{\text{cont}}$ ), and  $W_{\text{approx}}$ , computed using the definition of  $F_c$  suitable for the calibration process described in Sect. 4.4 ( $F_c = \bar{F}$ ). The percentage difference remains smaller than 20 per cent for almost all stars.

$(B - V)$ interval	$\Delta\lambda$ [Å]
$\leq 0.8$	14
$[0.8 - 1)$	16
$[1.0 - 1.2)$	20
$[1.2 - 1.3)$	24
$[1.3 - 1.5)$	28
$> 1.5$	40

**Table 3.** Wavelength window  $\Delta\lambda$  used in the calculation of the equivalent width for different values of  $(B - V)$  (see Equation 2).

the approximate definition of  $F_c$ , will be referred to as  $W_{\text{approx}}$ , and the one computed with  $F_{\text{cont}}$  will be referred simply as  $W_{\lambda}$ . The ratio between both values is plotted in Fig. 4. Again, using  $\bar{F}$  leads to an underestimation of the equivalent width. The differences are larger than for the continuum flux, but even in this case they remain smaller than 20 per cent.

## 4.2 Relation with colour index $(B - V)$

In Fig. 5 we illustrate the behaviour of  $W_{\lambda}$  as a function of the colour index  $(B - V)$ . In the y-axis we plot  $\log(W_{\lambda}/\lambda_o)$ , where  $\lambda_o = 5890$  Å. The small dots represent the mean value per star and the filled squares show the results of binning the data as explained in the previous section. As empty squares we plot the values of  $W_{\text{approx}}$ , binned in the same way.

A quadratic fit to the binned data gives

$$\log\left(\frac{W_{\lambda}}{\lambda_o}\right) = -4.579 + 1.948(B - V) - 0.3726(B - V)^2. \quad (3)$$

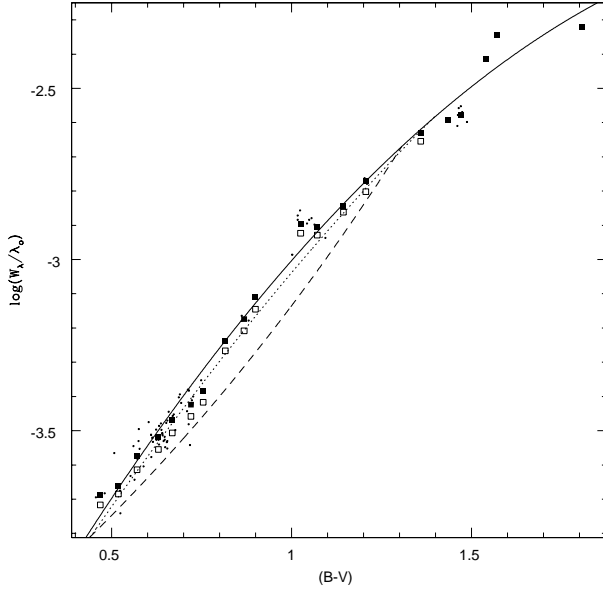


**Figure 5.** Equivalent width (logarithmic scale) vs  $(B - V)$ . The small dots are the mean values for each star and the filled squares are the mean values in each bin. The empty squares are the mean values of  $W_{approx}$  in each bin (see text). The solid line is the best fit to the binned data. The dotted line is the fit to  $W_{approx}$  and the dashed line is the fit given by Tripicchio et al., transformed to the colour index scale using Eq 5.

This fit is shown as a solid line in Fig. 5. It can be seen that, as the temperature decreases, the D lines become wider. It is evident from Fig. 5 that there is a saturation effect for the reddest stars. As shown in Fig. 1, for M stars with  $(B - V) \geq 1.4$ , the lines are so wide that they are almost completely blended. At this point, the doublet behaves as a single line, and the equivalent width grows mainly in the outer wings. Additionally, as cooler stars are also more active, the central line cores are filled in by chromospheric emission, contributing to the saturation effect.

### 4.3 Comparison

Tripicchio et al. (1997) also studied the dependence of the equivalent width with effective temperature. They constructed synthetic profiles of the D lines using a modified version of the MULTI code, which takes into account the line blending present in the doublet. They also observed a sample of dwarf and giant stars with spectral type between F6 and M5. They used both the modelled atmospheres and the observed spectra to obtain a relation between  $W_\lambda$  and effective temperature, given by:

$$\log\left(\frac{W_\lambda}{\lambda}\right) = 2.43 \cdot \frac{5040}{T_{eff}} - 5.73, \quad (4)$$

which reproduces their observations fairly well for effective temperatures higher than 4000 °K.

In order to compare this relation to our regression we performed a change of variables in equation 4 using the relation given by Noyes et al. (1984):

$$\log(T_{eff}) = 3.908 - 0.234 \cdot (B - V), \quad (5)$$

valid for stars with  $0.4 < (B - V) < 1.4$ . In this way we obtain  $W_\lambda$

as a function of  $(B - V)$ . The resulting expression is plotted as a dashed line in Fig. 5.

It can be seen that the values by Tripicchio et al. (1997) are smaller than ours: in some cases the difference between both expressions is as large as 40 per cent. Unfortunately, they do not mention how the continuum level or the integration windows were chosen. Although they say they used a wavelength interval of variable width and that they cleared the spectrum of unwanted lines, no details are given, so we could not apply their calculation method to our data.

To check whether our larger values of  $W_\lambda$  are due to the weak photospheric lines blended in the profiles, we recomputed the equivalent width in a completely different way, for several of our stars. We considered the raw spectra of 16 stars from our sample. The spectroscopic order in which the D lines are found was extracted, calibrated in wavelength and normalized. It is worth noting that the doublet is located in the middle of this order, where the effects of the blaze function are less severe. However, the presence of molecular bands prevented us from normalizing the spectra of M-type stars.

We then computed the equivalent width using the IRAF line-deblending routines included in the SPLOT task, which fit Voigt profiles to the lines, and perform the calculation over the fits. In this way, the presence of photospheric lines has no influence on the obtained value. Due to the severe blending of the D lines, the routine used by IRAF did not produce acceptable results for stars with colour larger than  $\approx 1.3$ . Therefore, this method can only be applied to stars with  $(B - V) < 1.3$ .

In Fig. 6 we plot as filled squares the value of  $W_\lambda$  calculated from our calibrated spectra Vs. the value obtained using IRAF ( $W_{IRAF}$ ). The errors in  $W_\lambda$  were calculated assuming a 3 per cent error in  $F_\lambda/F_c$  (see Eq. 2). The error bars in the x-axis were taken as the RMS of the fit done by IRAF times the width of the integration window (see Table 3). The solid line represents the identity relation, and not a fit to the data. It can be seen that the differences between our calculation and the one done with IRAF are well within the errors. The filled triangles represent the values of  $W_\lambda$  obtained from our fit, rather than from the individual observations. Note that the points still remain very close to the identity line.

As open squares we plot the equivalent width obtained from Tripicchio's relation (Eq. 4) for the value of  $(B - V)$  of the stars considered, which in all cases fall below the identity relation.

### 4.4 Determination of $(B - V)$

The relation shown in Fig. 5 can be used to determine the  $(B - V)$  of a star using the equivalent width of the D lines, measured in non-calibrated spectra. Since in many cases the spectral region needed to compute  $F_{cont}$  might fall outside the observed one, we repeat the fit for  $W_{approx}$ . The best least square fit to the binned values of  $\log(W_{approx}/\lambda_0)$  Vs.  $(B - V)$  is:

$$\log\left(\frac{W_{approx}}{\lambda_0}\right) = -4.528 + 1.734 (B - V) - 0.2442 (B - V)^2, \quad (6)$$

which is valid only for  $(B - V) < 1.4$ , and where  $\lambda_0 = 5890$  Å. This fit is plotted as a dotted line in Fig. 5.

To obtain  $(B - V)$  from the measured equivalent width, one could invert Eq. 6. However, since the least square estimation of parameters does not treat the dependent and independent variables symmetrically, a more rigorous procedure would be to fit  $(B - V)$  as a function of  $W_{approx}$ . We performed this fit and found that within the errors, both procedures give the same values of  $(B - V)$ .

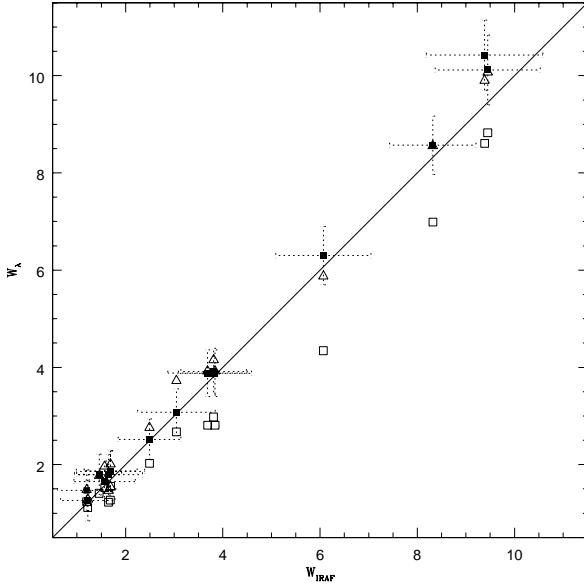


**Figure 6.**  $W_\lambda$  computed from the calibrated spectra (filled squares) as a function of the one given by the IRAF deblend routine ( $W_{\text{IRAF}}$ ). The triangles represent the values obtained from the fit of Eq. 3 and the empty squares represent the values obtained using the fit from Tripicchio et al. (1997).

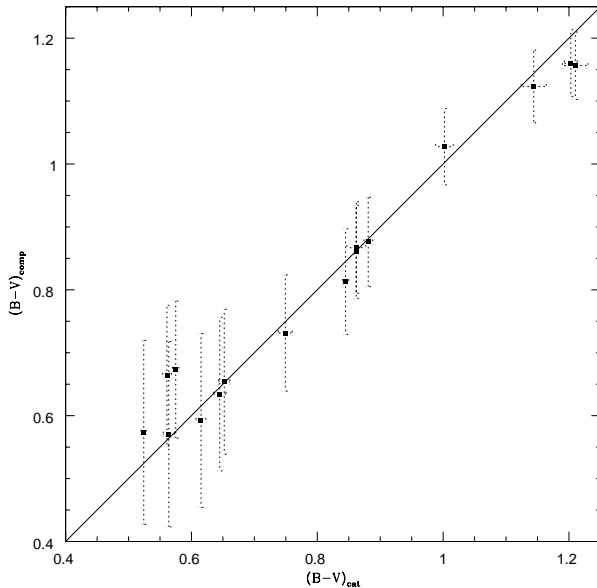


**Figure 7.**  $(B - V)$  computed from the normalized ([comp]) spectra through the inverse of Eq. 6 as a function of  $(B - V)$  from the Hipparcos/Tycho catalogue ([cat]). The solid line is the identity function. A good agreement is found between both values.

The method was verified using the same 16 stars used in the previous section. The raw spectra were extracted, calibrated in wavelength and normalized using Chebyshev polynomials. All these procedures were carried out using IRAF.  $W_\lambda$  was calculated by direct integration of the flux in the appropriate window (see Ta-

ble 3) using SPLOT. Then, the inverse of Eq. 6 was used to obtain  $(B - V)$  for these stars.

In Fig. 7 we plot the value of  $(B - V)$  computed in this way ( $(B - V)_{\text{comp}}$ ) as a function of the value obtained from the Hipparcos/Tycho catalogue ( $(B - V)_{\text{cat}}$ ). To estimate the error in  $(B - V)_{\text{comp}}$  we assumed a 5 per cent error in  $F_\lambda/F_c$ , in order to consider errors in the normalization procedure. The errors in the  $x$ -axis were taken from the Hipparcos/Tycho catalogue. The solid line represents the identity relation. It can be seen that the method gives, in fact, very good estimates of the colour of the stars.

Therefore, by measuring the equivalent width of the D doublet an estimate of the colour index  $(B - V)$  can be obtained. Afterwards, this value of  $(B - V)$  can be used to obtain an approximate flux calibration in the region of the D lines, by means of Eq. 1. In this way, the spectra of stars of unknown colour can be calibrated in flux in this spectral region.

## 5 ACTIVITY INDEXES AND CHROMOSPHERIC ACTIVITY

In this section, we define different activity indexes using the D lines, and study their applicability as chromospheric activity indicators.

### 5.1 N index

First, we constructed an index ( $N$ ) similar to the Mount Wilson  $S$  index, described by Vaughan et al. (1978).

$$N = \frac{f_1 + f_2}{f_{\text{cont}}},$$

where  $f_i$  is the mean flux in the  $D_i$  line, integrated in a square window 1 Å wide, and  $f_{\text{cont}}$  is the mean flux of the continuum calculated as explained in Sect. 3.1.

For the earlier stars in our sample, the  $N$  index is highly dependent on the colour  $(B - V)$ , as can be seen in Fig. 8. This behaviour changes for stars with  $(B - V) \gtrsim 1.1$ , for which the value of  $N$  is roughly constant. Stars with  $(B - V) < 1.1$  were fitted with a linear relation, shown in the figure as a solid line:

$$N_{(B-V)} = -1.584 \cdot (B - V) + 2.027. \quad (7)$$

In Fig. 9 we show the result of plotting  $N$  as a function of the  $S$  index, which was obtained from our spectra using the calibration presented in Cincunegui et al. (2006), which relates the  $S$  index obtained at CASLEO with the one computed at Mount Wilson. Note that since our spectra cover the entire visible range, we measure  $N$  and  $S$  simultaneously.

It can be seen that stars with  $(B - V) < 1.1$  (shown as filled triangles) have smaller values of  $S$ , and show a weak anticorrelation between  $N$  and  $S$  ( $r = -0.488$ ). We plot the observations for these stars alone in the upper panel of Fig. 10. Despite the considerable scatter, the anticorrelation is evident.

However, for these stars the correlation between  $N$  and  $(B - V)$  is stronger. To correct for this dependence we subtracted  $N_{(B-V)}$  (Eq. 7) from  $N$ . In the lower panel of Fig. 10 we plot  $N - N_{(B-V)}$  vs.  $(B - V)$ . In this case, the correlation disappears ( $r = 0.07$ ), implying that the correlation was due only to the dependence of  $N$  with colour, and the tendency of cooler stars to be more active. Therefore, the  $N$  index cannot be used as an activity indicator for stars with  $(B - V) < 1.1$ .

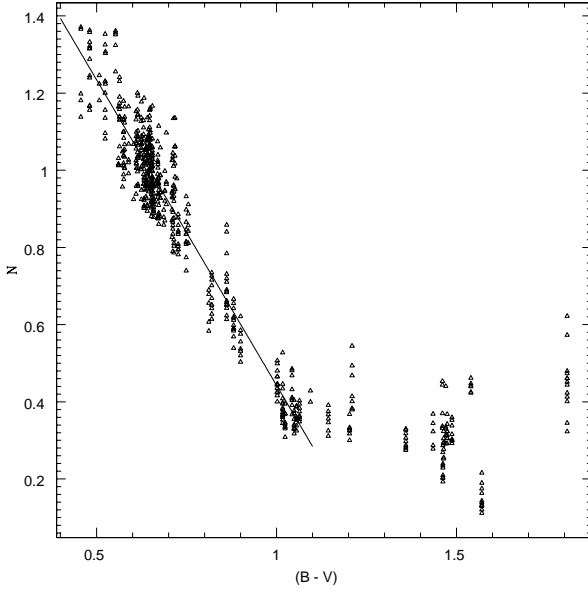


**Figure 8.** N index vs. colour index ( $B - V$ ). The solid line is the best linear fit for stars with  $(B - V) < 1.1$ . Stars with a larger  $(B - V)$  do not show any correlation.

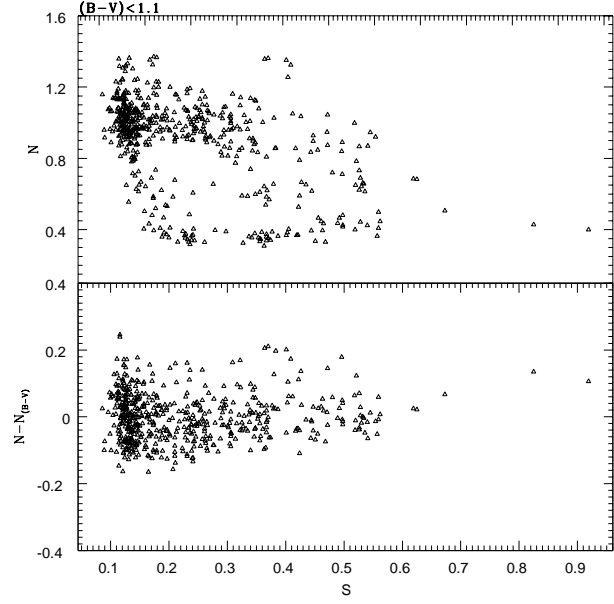


**Figure 10.** *Upper panel:* N vs. S for stars with  $(B - V) < 1.1$ . *Lower panel:* The dependence on N with colour has been corrected by subtracting  $N_{(B-V)}$ , shown in Eq. 7. The correlation disappears, as is confirmed by the small value of the correlation coefficient ( $r = 0.07$ ).

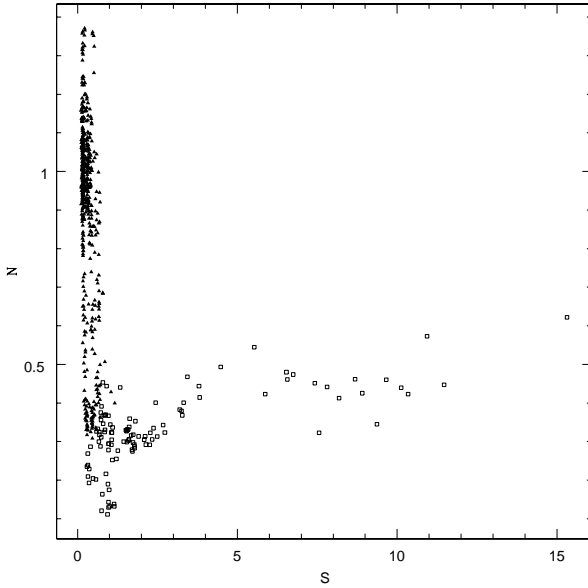


**Figure 9.** N vs. S. Values for stars with  $(B - V) < 1.1$  are shown as filled triangles, and those with  $(B - V) \geq 1.1$  as empty squares.

On the other hand, stars with  $(B - V) \geq 1.1$  present a good correlation between both N and S, as can be seen in Fig. 9. Since for these stars N do not correlate with colour, we do not perform any correction in this case.

Since we have simultaneous observations of both indexes, we can explore this apparent correlation for particular stars. In Fig. 11 we plot N vs S for several stars with  $(B - V) \geq 1.1$ , and we show the linear fits to each individual dataset (the slope of each fit is given in the legend). It can be seen that the slope of the relation be-

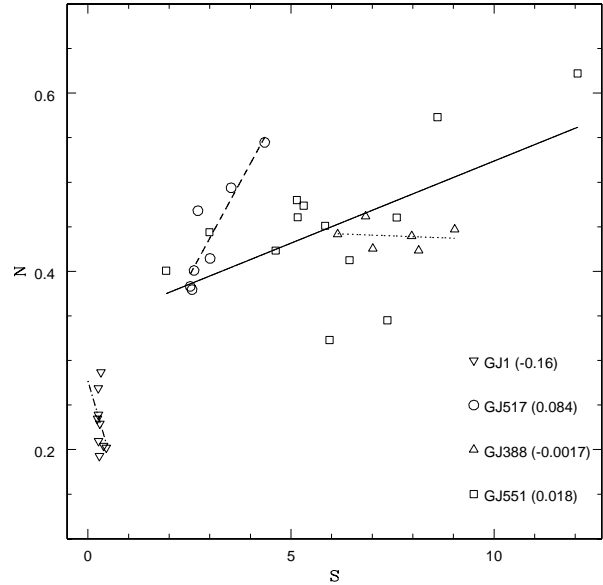


**Figure 11.** N vs S for selected stars with  $(B - V) \geq 1.1$ . A linear fit to the data of each star is also shown (GJ551: solid line; GJ388: dotted line; GJ517: dashed line; GJ1: dot-dash line). The slope of the fit is given in parentheses in the legend.

tween S and N changes from star to star, and the behaviour ranges from correlations with different slopes (GJ551 and GJ517) to cases where N and S are uncorrelated, either with constant S and variable N (GJ1) or viceversa (GJ388). A similar effect was observed comparing the flux of the  $H_\alpha$  line to the flux in the H and K lines (Cincunegui et al. 2006). In that case, we found correlations with

different slopes, anti-correlations, and cases where no correlation is present.

Therefore, the N index cannot be used to compare activity levels of different stars. However, it can be useful to compare activity levels on the *same* star at different times, for those stars which show a correlation between S and N. For example, N can be used to trace activity cycles in late-type stars, as we did with Proxima Centauri using the flux of the H $\alpha$  emission (see Cincunegui et al. 2007).

## 5.2 $R'_D$

Noyes et al. (1984, hereafter N84) noted that the S index is sensitive to the flux in the continuum windows and to the photospheric radiation present in the H and K bandpasses, both of which depend on spectral type. Despite the apparent independence of N with  $(B - V)$  seen in Fig. 8 for stars with  $(B - V) \geq 1.1$ , the results of the previous section seem to indicate that N also shows a dependence on photospheric flux, even for stars with  $(B - V) \geq 1.1$ . This dependence must be corrected more thoroughly in order to compare stars of different spectral type.

Following N84, we define a new index

$$R'_D = R_D - R_D^{phot}, \quad (8)$$

where  $R_D = (F_1 + F_2)/\sigma T_{eff}^4$ ,  $F_1$  and  $F_2$  are the fluxes in the D1 and D2 windows at the stellar surface, and  $\sigma$  is the Stefan-Boltzmann constant. Note that  $R_D$  can be expressed as:

$$R_D = \frac{f_1 + f_2}{f_{bol}} = \frac{f_{cont}}{f_{bol}} \cdot N, \quad (9)$$

where  $f_{bol}$  is the relative bolometric flux. Both expressions in Eq. 9 have the virtue of depending on fluxes on Earth instead of fluxes at the stellar surface.  $f_{bol}$  was computed interpolating the values of the bolometric correction provided by Johnson (1966). Defined in this way,  $R_D$  is independent of the photospheric flux in the continuum window.

$R_D^{phot}$  is the photospheric contribution to the flux in the windows of the D lines. For the H and K lines, N84 integrated the flux outside the H $_1$  and K $_1$  minima, and used these values to calculate  $R_{phot}$ , which is subtracted from  $R_{HK}$ . However, the D lines are usually in absorption. For this reason, we had to correct for the photospheric contribution in a different way. Since even for very inactive stars the D lines are not completely dark, the minimum line flux in a very inactive star must be photospheric in origin. Therefore, we assumed that the basal flux of the D lines is a reasonable estimation of the photospheric contribution.

In Fig. 12 we plot the flux in the D1 line as a function of the colour index  $(B - V)$ , in logarithmic scale. The solid line represents the basal flux, computed using a third order polynomial. The spectra with the D lines in emission were excluded from the fit. The resulting expression is:

$$\log(F_1^{min}) = -6.527 - 11.86 \cdot (B - V) + 10.87 \cdot (B - V)^2 - 4.218 \cdot (B - V)^3. \quad (10)$$

For the D2 line, a similar expression is obtained:

$$\log(F_2^{min}) = -6.374 - 12.48 \cdot (B - V) + 11.37 \cdot (B - V)^2 - 4.344 \cdot (B - V)^3. \quad (11)$$

Contrary to what happens for the H and K lines, this term is appreciable for all the range of our observations. Even for stars with Balmer lines in emission, the photospheric correction can be up to 50 per cent of the value of  $R_D$ .

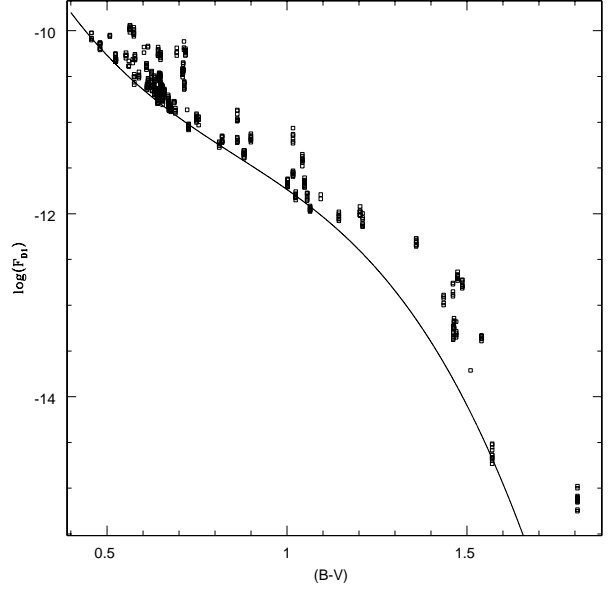


**Figure 12.** Flux in the D1 line as a function of colour index  $(B - V)$ . The solid line represents our estimation of the minimum flux. Those spectra with D lines in emission were not considered for the fit.

Following N84, we subtracted the same value of  $R_D^{phot}$  to all stars of the same spectral type. In this way, we have constructed an index eliminating the dependence on spectral type which arises from the photospheric flux in the integration bandpasses.  $R'_D$  should therefore depend exclusively on chromospheric flux and be independent of spectral type.

## 5.3 Chromospheric activity

According to N84,  $R'_{HK} = R_{HK} - R_{phot}$  is proportional to the fraction of nonradiative energy flux in the convective zone. Since this flux then heats the chromosphere by means of the magnetic field,  $R'_{HK}$  should be a good activity indicator.

We computed  $R'_{HK}$  for all our spectra using a relation analogue to Eq. 9. As  $R_{phot}$  we used the expression given in N84, valid in the range  $0.44 < (B - V) < 0.82$ ,

$$\log(R_{phot}) = -4.02 - 1.4 (B - V). \quad (12)$$

As noted by N84 the photospheric correction is unimportant for active stars. Indeed, we found that the correction is less than 10 per cent virtually for all stars with  $B - V > 1.1$ . Therefore, we used Eq. 12 for all the range of our observations.

To study its applicability as an activity indicator,  $R'_D$  was plotted against  $R'_{HK}$ . The result is presented in Fig. 13, where the filled triangles represent stars which exhibit the Balmer lines in emission. No correlation seems to be present when we consider the complete stellar sample. Indeed the correlation coefficient is  $r = 0.094$ . However, if we consider only the most active stars –those which exhibit Balmer lines in emission– an excellent correlation is found between both indexes. This is shown in Fig. 14, where we plot  $R'_D$  vs  $R'_{HK}$  only for these stars. The solid line is the best linear fit to the data:

$$R'_D = 2.931 \times 10^{-6} + 0.1388 \cdot R'_{HK}, \quad (13)$$

with correlation coefficient  $r = 0.978$ . This result demonstrates that

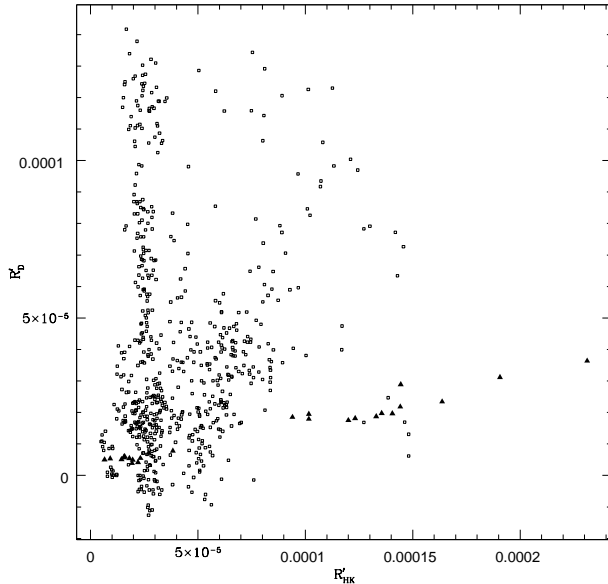


**Figure 13.**  $R'_D$  vs  $R'_{HK}$ . Filled triangles represent stars with Balmer lines in emission. No clear correlation is present, and the correlation coefficient for the complete sample is  $r = 0.094$ .

$R'_D$  can be used as an activity indicator for active stars. Note that despite presenting the Balmer lines in emission, not all stars in Fig. 14 present the D lines in emission, and this does not seem to be a condition for the use of  $R'_D$  as an activity indicator.  $R'_D$  is particularly useful to study the cooler stars, which tend to be more active and where the emission in the region of the H and K Ca II lines is substantially smaller (even an order of magnitude) than the flux in the region of the D doublet.

## 6 SUMMARY

A program was started in 1999 to study chromospheric activity and atmospheres of main sequence stars in the Southern Hemisphere. In this paper we analyze the sodium D lines. We use medium resolution *echelle* spectra, obtained in CASLEO, which were calibrated in wavelength and in flux.

We constructed an HR diagram for all the stars in our sample taking the colour index  $(B - V)$  and the visual magnitude  $V$  from the Hipparcos/Tycho catalogues. We found that several stars, in spite of being classified as dwarfs in the Simbad database, fall outside the main sequence. We present these stars in Table 1 and defer a more detailed analysis for future work. Conversely, in Table 2 we show four stars that were not classified as dwarfs even though they fall within the main sequence.

In Sect. 3 we define a pseudo-continuum level useful for all spectral types. Since in M stars the D lines are formed inside a TiO molecular band, we consider two windows located quite far from the doublet. In each window, the mean value of the ten highest points was calculated and the pseudo-continuum was defined as the linear interpolation between both windows. The continuum flux obtained in this way shows a very tight correlation with colour index  $(B - V)$ . Since most observations do not include regions too far from the lines, for stars with  $(B - V) < 1.4$  we also defined another pseudo-continuum, which uses a window located closer to the D

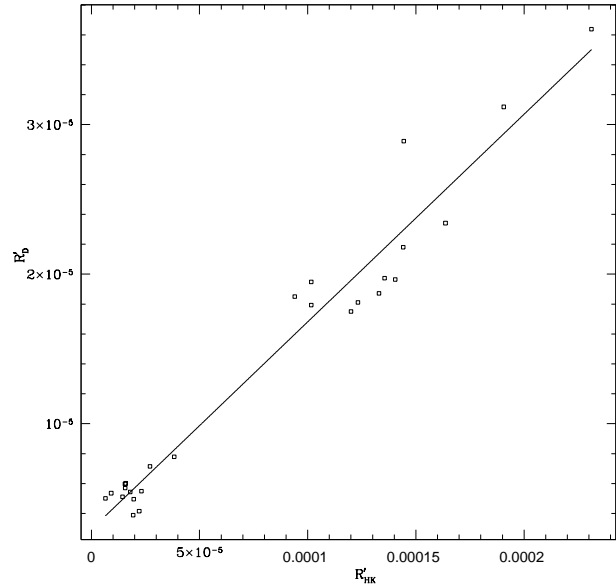


**Figure 14.**  $R'_D$  vs  $R'_{HK}$  for stars with Balmer lines in emission. The solid line is the best linear fit to the data, with correlation coefficient  $r = 0.977$ . The excellent correlation indicates that  $R'_D$  is a good chromospheric activity indicator.

lines, and also correlates strongly with  $(B - V)$ . We showed that this correlation can be used to obtain an approximate calibration in flux in this spectral region.

In Sect. 4 we describe in detail the computation of the equivalent width. We use a wavelength interval which range from 14 Å for F6 stars to 40 Å for the coolest stars in our sample. In M-type stars, the large photospheric wings, blended with deep molecular bands, difficult an accurate calculation. We find a good correlation between equivalent width and colour index  $(B - V)$  for all the range of observations.

The relation obtained was then used to determine the colour of dwarf-type stars from the equivalent width of the D lines. We find values of  $(B - V)$  in good agreement with those from the Hipparcos/Tycho catalogues. Since equivalent width is a characteristic of line profiles that do not require high resolution spectra to be measured, this fact could become a useful tool for subsequent studies.

Finally, in Sect. 5 we study how the flux in the D lines changes with changing levels of chromospheric activity. We define an index (N) analogue to Mount Wilson S index and find it is strongly correlated with colour for stars with  $(B - V) < 1.1$ . This fact produces an apparent correlation between N and S, which disappears when the colour dependence is taken into account. On the other hand, in stars with  $(B - V) \geq 1.1$ , N is independent of colour and is correlated with the S index. However, the slope between N and S varies when different stars are studied individually, varying from tight correlations to cases where no correlation is present. This fact restricts the use of the N index as an activity indicator when different stars are compared. However, the N index may be useful when comparing different activity levels on individual stars, specially in later stars with little emission in the region of the CaII H & K lines.

In order to compare activity levels on stars of different spectral types we define an improved index taking into account the photospheric contribution to the flux both in the lines and in the continuum windows. First we construct  $R_D$  as the ratio between absolute

line fluxes and stellar luminosity. Then, the photospheric contribution in the lines bandpasses, which was computed using the basal flux in the D lines, was subtracted from  $R_D$  to define  $R'_D$ . As was expected, the earlier stars in our sample do not show any sign of correlation between both indexes. Indeed, it has been known for a long time that the cores of the Na I D lines in the solar atmosphere remain dark from center to limb while the Ca II H&K lines show increasing line reversal. Only in stars with higher atomic densities, as the M-dwarfs, the D lines can be expected to have collision rates high enough to respond to the temperature changes in the chromosphere (e.g. Mauas 2000). Because of this, earlier theoretical works (see Andretta et al. 1997; Short & Doyle 1998) have restricted their attention to this type of stars. However, in this work the new  $R'_D$  index was found to correlate well with  $R'_{HK}$  for the most active stars in our sample (those which exhibit the Balmer lines in emission), even though some of these stars do not present a line reversal at the core of the D lines. Therefore,  $R'_D$  is also a good activity indicator for these stars. For the rest of the spectra, no correlation was found.

The CCD and data acquisition system at CASLEO has been partly financed by R. M. Rich through U.S. NSF grant AST-90-15827. This research has made use of the SIMBAD database, operated at CDS, Strasbourg, France. We thankfully acknowledge the comments and suggestions of the referee (Ian Short), which helped us to improve our original manuscript.

## REFERENCES

- Allen C. W., 1964, *Astrophysical Quantities*. Astrophysical Quantities, London: Athlone Press (2nd edition), 1964
- Andretta V., Doyle J. G., Byrne P. B., 1997, *A&A*, 322, 266
- Buccino A., Mauas P. J. D., 2007, *in preparation*
- Cayrel de Strobel G., Soubiran C., Friel E. D., Ralite N., Francois P., 1997, *A&AS*, 124, 299
- Cayrel de Strobel G., Soubiran C., Ralite N., 2001, *A&A*, 373, 159
- Cincunegui C., Díaz R. F., Mauas P. J. D., 2007, *A&A*, *in press*
- Cincunegui C., Díaz R. F., Mauas P. J. D., 2007, *A&A*, 461, 1107
- Cincunegui C., Mauas P. J. D., 2002, in *ESA SP-477: Solspa 2001*, Proceedings of the Second Solar Cycle and Space Weather Euroconference Cycles in other stars. pp 91–94
- Cincunegui C., Mauas P. J. D., 2004, *A&A*, 414, 699
- Henry T. J., Soderblom D. R., Donahue R. A., Baliunas S. L., 1996, *AJ*, 111, 439
- Hoeg E., Bässgen G., Bastian U., Egret D., Fabricius C., Großmann V., Halbwachs J. L., Makarov V. V., Perryman M. A. C., Schwekendiek P., Wagner K., Wicenec A., 1997, *A&A*, 323, L57
- Johnson H. L., 1966, *ARA&A*, 4, 193
- Mauas P. J. D., 2000, *ApJ*, 539, 858
- Mauas P. J. D., Falchi A., 1994, *A&A*, 281, 129
- Nordström B., Mayor M., Andersen J., Holmberg J., Pont F., Jørgensen B. R., Olsen E. H., Udry S., Mowlavi N., 2004, *A&A*, 418, 989
- Noyes R. W., Hartmann L. W., Baliunas S. L., Duncan D. K., Vaughan A. H., 1984, *ApJ*, 279, 763
- Perryman M. A. C., Lindegren L., Kovalevsky J., Hoeg E., Bastian U., Bernacca P. L., Crézé M., Donati F., Grenon M., van Leeuwen F., van der Marel H., Mignard F., Murray C. A., Le Poole R. S., Schrijver H., Turon C., Arenou F., Froeschlé M., Petersen C. S., 1997, *A&A*, 323, L49
- Short C. I., Doyle J. G., 1998, *A&A*, 336, 613
- Tripicchio A., Severino G., Covino E., Terranegra L., Garcia Lopez R. J., 1997, *A&A*, 327, 681
- Vaughan A. H., Preston G. W., Wilson O. C., 1978, *PASP*, 90, 267

**Table 4.** List of stars used in the analysis and average measurements. Nobs is the number of times the star has been observed.  $V$  is the visual magnitude in the UBV system.  $[\text{Fe}/\text{H}]$  is the iron abundance relative to the Sun, obtained from references (a): Cayrel de Strobel et al. (2001); (b): Nordström et al. (2004); (c): Cayrel de Strobel et al. (1997).  $\langle F_{\text{cont}} \rangle$  is the continuum flux (see Sect. 3.1).  $\langle \bar{F} \rangle$  is the mean flux in a window 20 Å wide around 5840 Å.  $\langle W_\lambda \rangle$  is the equivalent width of the sodium doublet and  $\langle W_{\text{approx}} \rangle$  is the equivalent width computed using  $\bar{F}$  as pseudo-continuum (see Sect. 4.1), in angstroms. Cols. 10 and 11 give the average absolute flux in a 1 Å window centered at the D1 and D2 lines, respectively. All fluxes are in units of  $[\text{erg cm}^{-2} \text{s}^{-1}]$ .  $\langle N \rangle$  is the value of the N index, calculated as explained in Sect. 5.1. Columns 13 and 14 give average value for the  $R_D$  index and the corresponding photospheric correction  $R_D^{\text{phot}}$  (see Sect. 5.2). Finally, in the last column we present the mean values of  $R'_{\text{HK}}$ . Colour index ( $B - V$ ), magnitude  $V$  and spectral type have been obtained from the Hipparcos/Tycho catalogues (Perryman et al. 1997; Hoeg et al. 1997).

Star	Nobs	Sp. type	$(B - V)$	$V$	$[\text{Fe}/\text{H}]$	$\langle F_{\text{cont}} \rangle$	$\langle \bar{F} \rangle$	$\langle W_\lambda \rangle$	$\langle W_{\text{approx}} \rangle$	$\langle F_{D1} \rangle$	$\langle F_{D2} \rangle$	$\langle N \rangle$	$\langle R_D \rangle$	$R_D^{\text{phot}}$	$\langle R'_{\text{HK}} \rangle$
hd28246	5	F6V	0.457	6.380	0.02 <sup>b</sup>	9.651e-12	9.591e-12	1.189	1.108	6.330e-12	5.739e-12	1.251	1.825e-04	1.761e-04	5.737e-05
hd38393	12	F7V	0.481	3.590	-0.12 <sup>a</sup>	1.293e-10	1.286e-10	1.222	1.153	8.595e-11	7.862e-11	1.272	1.897e-04	1.780e-04	3.084e-05
hd120136	3	F6IV	0.508	4.500	0.32 <sup>a</sup>	5.665e-11	5.618e-11	1.602	1.500	3.622e-11	3.270e-11	1.217	1.829e-04	1.037e-04	4.078e-05
hd16673	9	F6V	0.524	5.790	-0.01 <sup>a</sup>	1.711e-11	1.704e-11	1.243	1.192	1.098e-11	9.567e-12	1.201	1.784e-04	1.529e-04	4.929e-05
hd114762	3	F9V	0.525	7.300	-0.82 <sup>a</sup>	4.346e-12	4.325e-12	1.069	1.008	2.913e-12	2.641e-12	1.278	1.938e-04	1.716e-04	2.693e-05
hd35850	5	F7V	0.553	6.300	0.00 <sup>a</sup>	1.063e-11	1.057e-11	1.374	1.296	7.466e-12	6.673e-12	1.330	1.940e-04	1.198e-04	1.376e-04
hd17051	5	G0V	0.561	5.400	-0.04 <sup>a</sup>	2.536e-11	2.505e-11	1.679	1.526	1.423e-11	1.233e-11	1.047	1.582e-04	1.176e-04	4.635e-05
hd45067	11	F8V	0.564	5.880	-0.16 <sup>a</sup>	1.572e-11	1.562e-11	1.340	1.255	9.635e-12	8.603e-12	1.160	1.686e-04	4.831e-05	2.549e-05
hd52265	2	G0III-IV	0.572	6.290	0.21 <sup>a</sup>	1.108e-11	1.091e-11	1.541	1.347	5.911e-12	5.201e-12	1.003	1.490e-04	9.101e-05	2.567e-05
hd19994	9	F8V	0.575	5.070	0.15 <sup>a</sup>	3.438e-11	3.385e-11	1.736	1.543	1.932e-11	1.717e-11	1.062	1.587e-04	4.529e-05	3.132e-05
hd130948	6	G1V	0.576	5.860	-0.20 <sup>a</sup>	1.640e-11	1.622e-11	1.885	1.744	9.382e-12	8.210e-12	1.072	1.582e-04	1.445e-04	5.599e-05
hd75289	8	G0Ia	0.578	6.350	0.28 <sup>a</sup>	1.054e-11	1.039e-11	1.651	1.472	6.067e-12	5.247e-12	1.074	1.596e-04	8.565e-05	3.365e-05
hd215768	5	G0V	0.589	7.490	-0.20 <sup>b</sup>	3.678e-12	3.642e-12	1.466	1.342	2.083e-12	1.795e-12	1.054	1.550e-04	1.193e-04	6.666e-05
hd213240	2	G0/IV	0.603	6.810	0.13 <sup>b</sup>	6.975e-12	6.907e-12	1.975	1.856	3.737e-12	3.211e-12	0.996	1.484e-04	5.347e-05	2.894e-05
hd43587	7	F9V	0.610	5.700	-0.08 <sup>a</sup>	1.932e-11	1.908e-11	1.812	1.656	1.103e-11	9.575e-12	1.067	1.583e-04	8.101e-05	2.246e-05
hd197076	6	G5V	0.611	6.430	-0.20 <sup>b</sup>	9.906e-12	9.812e-12	1.560	1.440	5.488e-12	4.696e-12	1.028	1.533e-04	1.334e-04	2.160e-05
hd202996	2	G0V	0.614	7.460	0.00 <sup>b</sup>	3.735e-12	3.690e-12	1.778	1.629	2.355e-12	2.047e-12	1.179	1.711e-04	5.219e-05	6.028e-05
hd45270	6	G1V	0.614	6.530	-0.14 <sup>b</sup>	9.022e-12	8.913e-12	1.770	1.620	5.030e-12	4.464e-12	1.052	1.567e-04	1.141e-04	8.372e-05
hd165185	10	G5V	0.615	5.940	-0.06 <sup>a</sup>	1.540e-11	1.523e-11	1.727	1.589	8.778e-12	7.632e-12	1.066	1.573e-04	1.203e-04	6.079e-05
hd48189	6	G1.5V	0.624	6.150	-0.18 <sup>b</sup>	1.259e-11	1.248e-11	1.878	1.770	7.036e-12	6.370e-12	1.065	1.559e-04	8.756e-05	8.837e-05
hd147513	11	G5V	0.625	5.370	0.03 <sup>a</sup>	2.656e-11	2.618e-11	1.754	1.577	1.508e-11	1.271e-11	1.046	1.576e-04	1.201e-04	6.066e-05
hd150433	7	G0	0.631	7.210	-0.47 <sup>b</sup>	4.702e-12	4.649e-12	1.753	1.613	2.666e-12	2.294e-12	1.055	1.530e-04	1.185e-04	2.568e-05
hd219709	7	G2/3V	0.632	7.500	-0.02 <sup>a</sup>	3.607e-12	3.572e-12	1.925	1.808	1.922e-12	1.648e-12	0.990	1.438e-04	8.602e-05	4.212e-05
hd30495	11	G3V	0.632	5.490	-0.13 <sup>a</sup>	2.326e-11	2.304e-11	1.696	1.576	1.228e-11	1.047e-11	0.978	1.439e-04	1.187e-04	6.058e-05
hd202628	9	G2Va	0.637	6.750	-0.14 <sup>a</sup>	7.346e-12	7.261e-12	1.954	1.812	3.955e-12	3.401e-12	1.001	1.480e-04	1.141e-04	4.981e-05
hd38858	5	G4V	0.639	5.970	-0.25 <sup>b</sup>	1.511e-11	1.492e-11	1.872	1.710	8.241e-12	7.046e-12	1.011	1.498e-04	1.279e-04	2.778e-05
hd20766	12	G2.5V	0.641	5.530	-0.22 <sup>a</sup>	2.242e-11	2.225e-11	1.833	1.742	1.199e-11	9.930e-12	0.978	1.430e-04	1.384e-04	4.897e-05
hd59967	5	G4V	0.641	6.660	-0.19 <sup>b</sup>	8.012e-12	7.884e-12	1.826	1.629	4.420e-12	3.763e-12	1.021	1.512e-04	1.214e-04	7.739e-05
hd187923	10	G0V	0.642	6.160	-0.20 <sup>a</sup>	1.368e-11	1.350e-11	1.809	1.646	7.548e-12	6.660e-12	1.038	1.655e-04	4.708e-05	2.116e-05
hd19467	10	G3V	0.645	6.970	-0.13 <sup>b</sup>	5.923e-12	5.861e-12	1.736	1.607	3.277e-12	2.874e-12	1.039	1.508e-04	7.483e-05	2.271e-05
hd189567	8	G3V	0.648	6.070	-0.30 <sup>a</sup>	1.395e-11	1.377e-11	1.752	1.595	7.994e-12	6.906e-12	1.068	1.592e-04	1.008e-04	3.051e-05
hd210918	11	G5V	0.648	6.230	-0.18 <sup>a</sup>	1.154e-11	1.139e-11	1.788	1.623	6.353e-12	5.686e-12	1.043	1.491e-04	7.484e-05	2.604e-05
hd173560	9	G3/5V	0.649	8.690	-0.21 <sup>b</sup>	1.272e-12	1.248e-12	1.667	1.427	7.344e-13	6.385e-13	1.079	1.637e-04	4.757e-05	3.793e-05
hr6060	15	G2Va	0.652	5.490	0.05 <sup>a</sup>	2.369e-11	2.331e-11	1.962	1.765	1.221e-11	1.033e-11	0.951	1.408e-04	9.134e-05	2.526e-05
hd11131	9	G0	0.654	6.720	-0.06 <sup>a</sup>	7.558e-12	7.474e-12	1.726	1.587	4.098e-12	3.439e-12	0.997	1.460e-04	1.038e-04	7.184e-05
hd20619	11	G1.5V	0.655	7.050	-0.20 <sup>a</sup>	5.339e-12	5.293e-12	1.738	1.632	2.916e-12	2.486e-12	1.012	1.417e-04	1.212e-04	3.218e-05
hd217343	2	G3V	0.655	7.470	-0.18 <sup>b</sup>	3.768e-12	3.711e-12	1.995	1.810	2.075e-12	1.805e-12	1.030	1.499e-04	1.060e-04	1.057e-04
hd4308	12	G5V	0.655	6.550	-0.47 <sup>a</sup>	8.907e-12	8.808e-12	1.652	1.513	4.651e-12	3.991e-12	0.970	1.431e-04	9.757e-05	2.719e-05
hd1835	13	G3V	0.659	6.390	-0.01 <sup>a</sup>	1.067e-11	1.049e-11	2.116	1.921	5.225e-12	4.551e-12	0.917	1.393e-04	9.379e-05	6.410e-05
hd213941	9	G5V	0.670	7.580	-0.42 <sup>a</sup>	3.335e-12	3.313e-12	2.057	1.977	1.759e-12	1.508e-12	0.979	1.386e-04	1.031e-04	3.985e-05

Table 4 – continued

Star	Nobs	Sp. type	(B – V)	V	[Fe/H]	< $F_{cont}$ >	< $\bar{F}$ >	< $W_\lambda$ >	< $W_{approx}$ >	< $F_{D1}$ >	< $F_{D2}$ >	< N >	< $R_D$ >	$R_D^{phot}$	< $R'_{HK}$ >
hd197214	10	G5V	0.671	6.950	-0.5 <sup>b</sup>	6.138e-12	6.048e-12	1.983	1.804	3.224e-12	2.719e-12	0.968	1.411e-04	1.186e-04	3.608e-05
hd172051	13	G5V	0.673	5.850	-0.29 <sup>b</sup>	1.699e-11	1.677e-11	2.078	1.923	8.668e-12	7.367e-12	0.944	1.380e-04	1.266e-04	2.725e-05
hd19034	8	G5	0.677	8.080	-0.39 <sup>b</sup>	2.167e-12	2.148e-12	1.870	1.767	1.128e-12	9.443e-13	0.957	1.389e-04	1.297e-04	2.861e-05
hd203019	3	G5V	0.687	7.840	0.07 <sup>b</sup>	2.710e-12	2.652e-12	2.330	2.078	1.256e-12	1.123e-12	0.878	1.272e-04	9.105e-05	9.492e-05
hd202917	5	G5V	0.690	8.650	-0.16 <sup>b</sup>	1.269e-12	1.250e-12	2.377	2.198	6.377e-13	5.505e-13	0.936	1.338e-04	1.183e-04	1.416e-04
hd12759	4	G3V	0.694	7.300	-0.13 <sup>b</sup>	4.585e-12	4.501e-12	2.245	2.026	2.427e-12	2.093e-12	0.986	1.465e-04	2.882e-05	7.779e-05
hd128620	7	G2V	0.710	-0.010	0.22 <sup>a</sup>	3.844e-09	3.777e-09	2.123	1.912	1.943e-09	1.591e-09	0.919	1.355e-04	4.082e-05	2.221e-05
hd41824	11	G6V	0.712	6.600	-0.09 <sup>b</sup>	9.098e-12	8.924e-12	2.456	2.231	4.401e-12	3.864e-12	0.909	1.394e-04	3.642e-05	1.074e-04
hd117176	3	G4V	0.714	4.970	-0.11 <sup>a</sup>	3.835e-11	3.783e-11	1.947	1.780	2.074e-11	1.897e-11	1.036	1.492e-04	2.157e-05	1.581e-05
hd34443	9	K1V	0.715	5.570	-0.16 <sup>c</sup>	2.212e-11	2.186e-11	2.440	2.305	1.051e-11	8.790e-12	0.872	1.259e-04	5.059e-05	2.837e-05
hd3795	9	G3/5V	0.718	6.140	-0.70 <sup>a</sup>	1.299e-11	1.288e-11	1.692	1.584	7.208e-12	6.159e-12	1.029	1.472e-04	2.478e-05	2.282e-05
hd203244	1	G5V	0.723	6.980	-0.21 <sup>a</sup>	6.150e-12	6.069e-12	2.284	2.128	3.265e-12	2.754e-12	0.979	1.434e-04	1.010e-04	7.445e-05
hd10700	11	G8V	0.727	3.490	-0.59 <sup>a</sup>	1.490e-10	1.475e-10	2.344	2.227	6.720e-11	5.630e-11	0.829	1.180e-04	1.243e-04	3.117e-05
hd152391	11	G8V	0.749	6.650	-0.06 <sup>b</sup>	8.579e-12	8.407e-12	2.613	2.379	3.882e-12	3.263e-12	0.833	1.238e-04	9.103e-05	6.268e-05
hd36435	5	G6/8V	0.755	6.990	-0.02 <sup>a</sup>	6.071e-12	5.984e-12	2.425	2.255	2.798e-12	2.433e-12	0.862	1.235e-04	8.948e-05	6.689e-05
hd13445	5	K1V	0.812	6.120	-0.21 <sup>a</sup>	1.365e-11	1.338e-11	3.400	3.147	4.822e-12	3.947e-12	0.643	8.931e-05	8.795e-05	3.455e-05
hd26965	10	K1V	0.820	4.430	-0.25 <sup>a</sup>	6.876e-11	6.776e-11	3.413	3.228	2.547e-11	2.081e-11	0.673	9.885e-05	8.235e-05	2.275e-05
hd177996	9	K1V	0.862	7.890	-0.28 <sup>b</sup>	2.876e-12	2.798e-12	4.034	3.699	1.131e-12	9.836e-13	0.735	1.048e-04	3.767e-05	7.872e-05
hd17925	7	K1V	0.862	6.050	0.10 <sup>a</sup>	1.648e-11	1.608e-11	3.898	3.596	5.892e-12	4.904e-12	0.655	9.825e-05	6.478e-05	8.305e-05
hd22049	13	K2V	0.881	3.720	-0.14 <sup>a</sup>	1.318e-10	1.292e-10	3.905	3.653	4.355e-11	3.628e-11	0.606	8.335e-05	6.921e-05	5.299e-05
hd128621	8	K1V	0.900	1.350	0.24 <sup>a</sup>	1.220e-09	1.183e-09	4.576	4.216	3.709e-10	3.049e-10	0.554	7.802e-05	3.906e-05	2.154e-05
gl349	12	K3V	1.002	7.200	-0.15 <sup>b</sup>	5.535e-12	5.373e-12	6.086	5.667	1.353e-12	1.142e-12	0.451	5.558e-05	4.579e-05	5.335e-05
gl542	9	K3V	1.017	6.660	0.26 <sup>a</sup>	9.770e-12	9.361e-12	7.693	7.154	1.959e-12	1.678e-12	0.372	4.834e-05	2.846e-05	1.566e-05
hd188088	6	K3/4V	1.017	6.220	–	1.499e-11	1.433e-11	7.920	7.369	3.456e-12	2.903e-12	0.425	5.636e-05	1.315e-05	4.730e-05
hd131977	9	K4V	1.024	5.720	0.03	2.381e-11	2.322e-11	8.199	7.903	4.477e-12	3.802e-12	0.348	4.588e-05	4.552e-05	2.660e-05
gl610	9	K3/4V	1.043	7.390	-0.03 <sup>a</sup>	4.892e-12	4.719e-12	7.510	7.054	1.128e-12	9.638e-13	0.428	5.266e-05	1.849e-05	1.505e-05
hd32147	10	K3V	1.049	6.220	0.34 <sup>a</sup>	1.468e-11	1.415e-11	7.691	7.232	2.773e-12	2.353e-12	0.349	4.360e-05	2.653e-05	1.978e-05
gl845	8	K4.5V	1.056	4.690	-0.23 <sup>a</sup>	6.041e-11	5.768e-11	7.782	7.203	1.179e-11	1.008e-11	0.362	4.505e-05	3.618e-05	2.748e-05
gl435	8	K4/5V	1.064	7.770	–	3.576e-12	3.467e-12	7.456	7.062	7.230e-13	6.108e-13	0.373	4.640e-05	4.852e-05	2.499e-05
hd216803	2	K4V	1.094	6.480	–	1.181e-11	1.159e-11	6.814	6.562	2.636e-12	2.258e-12	0.414	4.993e-05	3.080e-05	6.597e-05
hd156026	7	K5V	1.144	6.330	-0.21 <sup>a</sup>	1.398e-11	1.357e-11	8.456	8.105	2.623e-12	2.313e-12	0.353	4.114e-05	2.798e-05	3.156e-05
gl416	7	K4V	1.203	9.060	–	1.178e-12	1.121e-12	10.178	9.482	2.018e-13	1.851e-13	0.329	3.623e-05	1.301e-05	2.745e-05
gl517	7	K5Ve	1.210	9.240	-0.15 <sup>c</sup>	9.272e-13	8.849e-13	9.795	9.116	2.115e-13	1.972e-13	0.441	4.464e-05	1.877e-05	1.643e-04
hd157881	9	K5	1.359	7.540	-0.20 <sup>a</sup>	5.122e-12	4.868e-12	13.782	13.040	8.167e-13	7.218e-13	0.300	2.634e-05	3.709e-06	3.227e-05
gl526	5	M1.5	1.435	8.460	–	2.297e-12	–	15.084	–	3.925e-13	3.433e-13	0.320	2.379e-05	4.811e-06	1.880e-05
gl536	5	M1	1.461	9.710	–	7.087e-13	–	14.472	–	1.436e-13	1.307e-13	0.387	2.547e-05	2.607e-06	1.920e-05
gl1	9	M1.5	1.462	8.560	–	2.062e-12	–	15.579	–	2.574e-13	2.163e-13	0.230	1.520e-05	4.825e-06	6.587e-06
hd180617	8	M2.5	1.464	9.120	–	1.220e-12	–	16.324	–	1.837e-13	1.661e-13	0.287	1.866e-05	4.279e-06	2.185e-05
gl479	6	M2	1.470	10.650	–	3.116e-13	–	16.527	–	5.484e-14	5.032e-14	0.338	2.246e-05	5.738e-06	3.258e-05
hd36395	8	M1.5	1.474	7.970	0.60 <sup>c</sup>	3.719e-12	–	15.876	–	6.313e-13	5.648e-13	0.322	2.133e-05	1.291e-06	4.688e-05
hd42581	8	M1/2V	1.487	8.150	–	3.000e-12	–	14.864	–	5.104e-13	4.495e-13	0.320	1.895e-05	1.113e-06	2.533e-05
gl388	6	M3.5Ve	1.540	9.430	–	9.761e-13	–	22.636	–	2.003e-13	2.289e-13	0.440	1.987e-05	1.501e-06	1.122e-04
gl699	11	M4Ve	1.570	9.540	–	9.174e-13	–	26.649	–	7.240e-14	6.531e-14	0.150	4.653e-06	4.012e-06	1.006e-05
gl551	13	M5.5Ve	1.807	11.010	–	2.303e-13	–	28.131	–	4.582e-14	5.835e-14	0.452	5.566e-06	2.657e-08	1.883e-05